Journal of Colloid and Interface Science 349 (2010) 505–511

Contents lists available at ScienceDirect

Journal of Colloid and Interface Science

www.elsevier.com/locate/jcis

Improved photoluminescence properties of a novel europium(III) complex covalently grafted to organically modified silicates

Yinghui Wang [a,b], Bin Li [a,*], Liming Zhang [a,b], Qinghui Zuo [a,b], Lina Liu [a,b], Peng Li [a,b]

[a] Key Laboratory of Excited State Processes, Changchun Institute of Optics, Fine Mechanics and Physics, Chinese Academy of Sciences, 3888 Eastern South-Lake Road, Changchun 130033, People's Republic of China
[b] Graduate School of the Chinese Academy of Sciences, Chinese Academy of Sciences, Beijing 100039, People's Republic of China

ARTICLE INFO

Article history:
Received 2 March 2010
Accepted 14 May 2010
Available online 20 May 2010

Keywords:
ORMOSILs
Covalently grafted
Europium(III) complex
Photoluminescence

ABSTRACT

A series of novel organic–inorganic hybrid materials with a Eu(III) complex $[(C_2H_5)_4N][Eu(DBM)_3(DBM\text{-}OH)]$ (DBM = dibenzoylmethanate, DBM-OH = *p*-hydroxydibenzoylmethanate) covalently bonded into vinyl-modified silica networks have been successfully assembled through a sol–gel process. DBM-OH was grafted to the coupling agent 3-(triethoxysilyl)propylisocyanate (TESPIC), and the as-obtained molecular precursor DBM-Si was used as a bridge molecule both coordinate to Eu^{3+} and forming an inorganic Si–O network with tetraethoxysilane (TEOS) and vinyltriethoxysilane (VTES) after cohydrolysis and co-condensation processes. The luminescence properties of VTES/TEOS composite hybrid materials were systematically studied in comparison to those of TEOS-derived hybrid material and pure $[(C_2H_5)_4N][Eu(DBM)_4]$, respectively. The results indicate that the luminescent quantum efficiencies of VTES/TEOS composite hybrid materials are greatly improved. And it is interesting to find that the luminescent intensity of VTES/TEOS composite hybrid material is enhanced by optimizing the molar ratio of VTES to TEOS (VTES:TEOS = 4:6) by 3.3 and 2.4 times compared with TEOS-derived hybrid material and pure $[(C_2H_5)_4N][Eu(DBM)_4]$, respectively. In addition, the thermal stability of the emission was also improved considerably. The results presented in this paper indicate that the use of vinyl-modified silicates as a matrix opens the door to improving the photoluminescence properties of Eu(III) complexes.

1. Introduction

Rare-earth (RE) complexes are well known for their excellent luminescence properties, e.g., extremely sharp emission peaks, long lifetimes, and potential high internal quantum efficiency, which are due to effective intramolecular energy transfers from the coordinated ligands to the luminescent central lanthanide ions [1–3]. Some RE complexes demonstrate potential applications in fluoroimmunoassays, lasers, optical amplification, and organic light-emitting diodes [4–8]. However, their poor stability under high temperature and moisture and low mechanical strength restrict their practical applications.

A promising way to overcome these shortcomings is the use of the sol–gel method or the hydrothermal synthesis process to incorporate RE complexes into an inert matrix, such as inorganic and organic–inorganic hybrid matrices [9–16]. Organic–inorganic hybrid materials combine some advantages of organic compounds (easy processing with conventional techniques, elasticity, and organic functionalities) with properties of inorganic oxides (hardness, thermal and chemical stability, transparency); therefore they can exhibit excellent mechanical properties and good thermal and photostability [17–20]. Organically modified silicates (ORMOSILs) are one kind of organic–inorganic hybrid matrices with many excellent properties, such as low brittleness, considerable flexibility, and elasticity, with respect to traditional silica xerogels, and exhibit tremendous potential applications in optics, electrics, biology, and catalysis [21–24]. A typical process for preparing ORMOSILs is cohydrolysis and co-condensation from a mixture of a tetralkoxysilane and an alkyl-substituted silicon alkoxides. The nonreactive organic groups do not undergo hydrolysis or condensation, remaining unaltered during the sol–gel process and acting as a network modifier that terminates the silicate networks. Because the interconnection of organic and inorganic moieties in this network results in microstructure changes, improvement of density, flexibility, and optical properties has been achieved, making ORMOSILs more suitable as matrices for a range of applications. Recently, the use of ORMOSILs as a support has been of widespread interest in optical oxygen sensors [25–29]. However, only limited examples of using vinyl-modified silicates as matrices for Eu(III) complexes have been reported [30–32], and these studies were mainly focused on vinyl-modified silicate

* Corresponding author. Fax: +86 431 86176935.
E-mail address: lib020@yahoo.cn (B. Li).

0021-9797/$ - see front matter © 2010 Elsevier Inc. All rights reserved.
doi:10.1016/j.jcis.2010.05.047

matrices doped with the Eu(III) complexes in which only weak physical interactions exist between the Eu(III) complexes and the matrices. Up to date, as far as we know, the synthesis and luminescence properties of vinyl-modified silicate matrices covalently bonded with Eu(III) complexes have not been explored.

Here, we report on the synthesis of a series of organic–inorganic hybrid materials covalently bonded with a novel Eu(III) complex $[(C_2H_5)_4N][Eu(DBM)_3(DBM\text{-}Si)]$ (depicted in Fig. 1) by a sol–gel process using ORMOSILs as matrices, in which VTES was selected as an organic modifier in the precursor. It is interesting that the luminescent intensity and emission quantum efficiency of these VTES/TEOS composite hybrid materials showed strong dependence on the molar ratio of VTES to TEOS. The luminescent intensity of VTES/TEOS composite hybrid material is enhanced by optimizing the molar ratio of VTES to TEOS (VTES:TEOS = 4:6) by 3.3 and 2.4 times compared with TEOS-derived hybrid material and pure $[(C_2H_5)_4N][Eu(DBM)_4]$, respectively. In addition, the thermal stability of the emission is also improved considerably.

2. Materials and methods

2.1. Materials

Tetraethoxysilane (TEOS, Tianjin Chemicals Co.), 3-(triethoxysilyl)-propyl isocyanate (TESPIC, Aldrich), vinyltriethoxysilane (VTES, Tianjin Chemicals Co.), acetophenone (Tianjin Chemicals Co.), *p*-hydroxybennic acid (Tianjin Chemicals Co.), tetraethylammonium bromide (Tianjin Chemicals Co.), and dibenzoylmethane (DBM, Aldrich) were used as received. The solvent tetrahydrofuran (THF) was used after desiccation with anhydrous calcium chloride. Europium chloride ($EuCl_3$) was prepared by dissolving Eu_2O_3 in concentrated hydrochloric acid (HCl).

2.2. Synthetic procedures

2.2.1. Synthesis of p-hydroxydibenzoylmethane (DBM-OH)

DBM-OH was prepared using a Claisen condensation between *p*-hydroxybenzoate and acetophenone in the presence of sodium

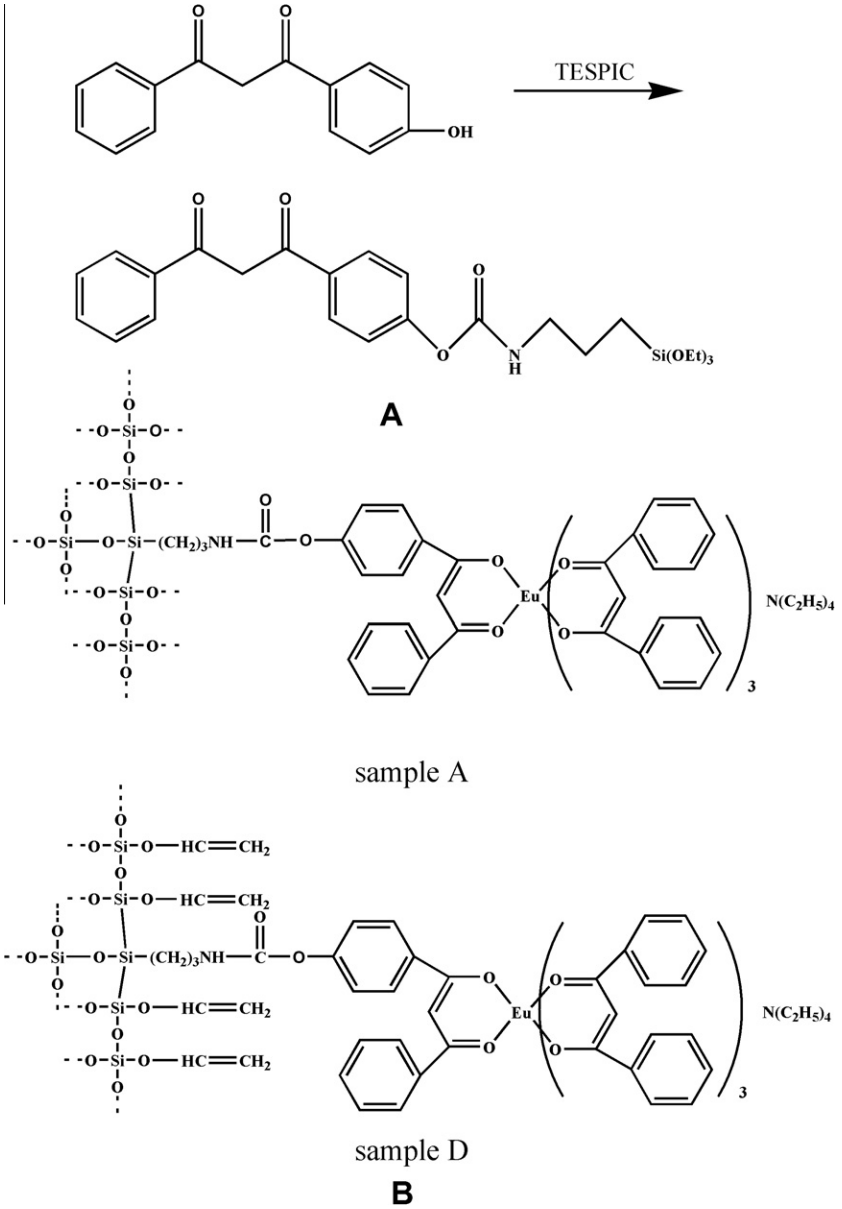

Fig. 1. Synthetic procedures of the silylated precursor DBM-Si(A) and the predicted structure of xerogels containing Eu(III) complex.

hydride. After being refluxed in anhydrous THF at 90 °C for 12 h, the mixture was acidified by hydrochloric acid to pH 2–3. The solid product was filtered off and then purified by silica column chromatography to give DBM-OH with a yield of 42%. ^{1}H NMR ($CDCl_3$, 400 MHz) δ (ppm): 12.43 (1H, s), 10.22 (1H, s), 7.79–7.76 (4H, m), 6.83–6.79 (5H, m), 6.02 (1H, s). Anal. Calcd. for $C_{15}H_{12}O_3$: C, 75.00; H, 5.00. Found: C, 74.89; H, 5.09.

2.2.2. Synthesis of Eu(III) complex functionalized VTES/TEOS composite hybrid materials

A typical procedure for the preparation of the modified precursor DBM-Si has been described elsewhere [33] and can be summarized as follows: DBM-OH (0.24 g; 10 mmol) was mixed with an excess of TESPIC (10 ml; 37.5 mmol) in a round-bottom flask, and then the mixture was kept under nitrogen in an ultrasonic bath for about 30 min. The mixture was stirred at 80 °C for 72 h. After isolation and purification, a white–yellow solid sample of DBM-Si was obtained. DBM-Si: IR –OH 3392 cm^{-1}, –CONH– 1695 cm^{-1}, $-(CH_2)_3-$ 2942 cm^{-1}, Si–O 1080 cm^{-1}. Then the pure TEOS-derived xerogel was prepared by resolving DBM-Si and DBM in dimethylformamide (DMF) with stirring. A stoichiometric amount of $EuCl_3$ was added to the solution. After 2 h, a corresponding amount of TEOS was added to the reaction solution. Then one drop of diluted hydrochloric acid was put into it to promote hydrolysis. The mole ratio of Eu^{3+}/DBM/DBM-Si/TEOS/H_2O was 1:3:1:12:48. The mixture was agitated magnetically to achieve a single phase in a covered Teflon beaker, and then it was aged at 80 °C until the onset of gelation. The gels were collected as transparent crack-free monolithic bulks and ground as a solid powder material (denoted as sample A) for the photophysical studies. The synthetic procedure of VTES/TEOS composite xerogels was similar to the above preparation of TEOS-based xerogel with some minor modifications by mixing TEOS and VTES together to form solutions that contained 20, 40, and 60 mol% VTES (denoted as samples B, C, and D, respectively).

2.2.3. Synthesis of $Gd(DBM\text{-}Si)_3{\cdot}2H_2O$ complex

$Gd(DBM\text{-}Si)_3{\cdot}2H_2O$ was prepared according to the following procedure: 3 mmol of DBM-Si was dissolved in a certain amount of anhydrous ethanol at room temperature, and then 1 mmol of $GdCl_3$ ethanol solution was added under stirring for 5 h. The yellow powder was filtered and washed with ethanol. The obtained $Gd(DBM\text{-}Si)_3{\cdot}2H_2O$ was dried at 60 °C under vacuum overnight.

2.3. Characterization

The FT-IR spectra were recorded within the region 400–4000 cm^{-1} using an FT-IR spectrophotometer (Bruker Vertex Model 70 FTIR) with a resolution of ±4 cm^{-1} using the KBr pellet technique. ^{1}H NMR spectra were recorded on a Bruker AC 400 spectrometer. CHN elemental analysis was performed on a 240 Perkin–Elmer analyzer. Absorption spectra were measured using a UV–vis spectrophotometer (Shimadzu, UV-3100). Thermogravimetric analysis (TGA) was performed on 2 mg of samples using a Perkin–Elmer thermal analyzer. The samples were heated from 40 to 600 °C at a heating rate of 10.0 °C/min. A 10-ml/min flow of dry nitrogen was used to purge the sample at all times. Excitation and emission spectra were recorded at room temperature using a Hitachi F-4500 spectrophotometer equipped with a continuous 150-W Xe-arc lamp. In the measurements of temperature dependence of fluorescence, the samples were placed in a liquid nitrogen cycling system (pellet). A continuous 325-nm light from a He–Cd laser was used as the excitation source. The fluorescence was measured by a UV-Lab Raman Infinity (made by Jobin Yvon Company) with a resolution of 2 cm^{-1}. In the measurements of fluorescence dynamics, a 355-nm light generated from the Nd^{3+}:YAG laser combined with a fourth harmonic generator was used as the pump, with a repetition frequency of 10 Hz and a pulse duration of 10 ns. A two-channel TEKTRONIX TDS-3052 oscilloscope was used to record fluorescence decay curves.

3. Results and discussion

As detailed in Section 2, the successful covalent grafting of DBM-OH to the coupling agent TESPIC is supported by the FT-IR spectra. The IR spectra for DBM-OH (a) and DBM-Si (b) are shown in Fig. 2I. The absorption band at 3392 cm^{-1} in Fig. 2Ia corresponds to the strong vibration of hydroxyl. The emergence of a series of bands at 2979, 2942, and 2887 cm^{-1} due to the vibrations of methylene $-(CH_2)_3-$ and the disappearance of the stretch vibration of the absorption peaks at 2250–2275 cm^{-1} for N=C=O of TESPIC in Fig. 2Ib indicate that DBM-OH has been successfully grafted onto TESPIC.

All of the hybrid materials obtained were also characterized by infrared spectroscopy. The FT-IR spectra of TEOS-based xerogel (A) and VTES/TEOS composite xerogels (B–D) are presented in Fig. 2II. The formation of the Si–O–Si framework is evidenced by the bands of absorption of siloxane bonds located at 1080 (ν_{as}, Si–O), 796 (ν_s, Si–O), and 468 cm^{-1} (δ, Si–O–Si) (ν represents stretching, δ in plane bending, s symmetric, and as asymmetric vibrations) in Figs. 2IIA–2IID [34]. The ν (Si–C) vibrations located at 1208–1198 cm^{-1} are still observed in the IR spectra of all the materials, which is consistent with the fact that the Si–C bond is reserved during reactions. In addition, vibration peaks near 3065 cm^{-1} (originating from Si–CH=CH_2) appear in Figs. 2IIB–2IID, which are not found in Fig. 2IIA, suggesting the presence of vinyl in the ORMOSILs.

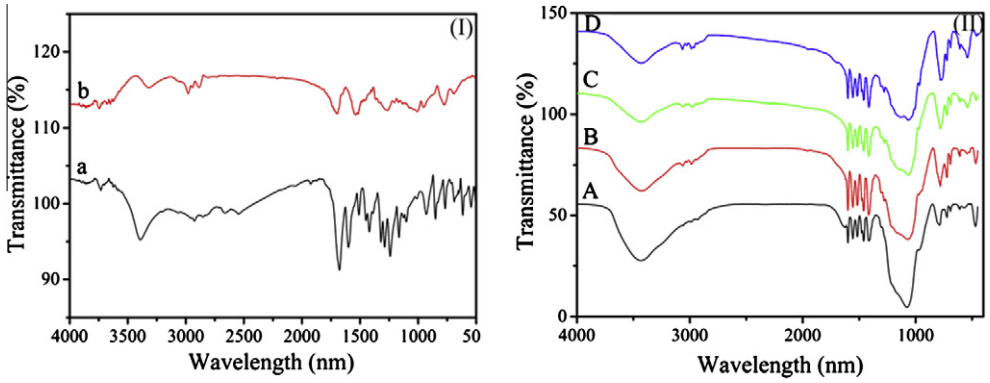

Fig. 2. Infrared spectra of (I) DBM-OH (a) and DBM-Si (b) and (II) TEOS-based xerogel (A) and VTES/TEOS composite xerogels (B–D) in the 4000–400 cm^{-1} range.

Furthermore, compared with Fig. 2IIA–2IID, the intensity ratio of the adsorption peaks located near 3065 cm^{-1} (assigned to the Si–CH=CH_2 vibration) to the broad peak near 3400 cm^{-1} (assigned to the Si–OH vibration) was found to increase from A to D, indicating that Si–CH=CH_2 groups replace the surface Si–OH groups, and their number increases with increasing addition of VTES in the bulk xerogels.

UV–vis absorption spectra of DBM-Si and the samples (A–D) are shown in Fig. 3. From the spectra, it is observed that there was a blue shift (from 258 to 247 nm, Δv = 11 nm) between the precursor DBM-Si and the samples A–D. This may be attributed to the coordination interaction between the Eu^{3+} ion and DBM-Si, which enlarges the energy levels of the major π–π* transition and thus exhibits an obvious blue shift [35]. UV–vis absorption spectra for all the samples exhibit a broad absorption band in the UV–vis region (200–450 nm). This absorption band is assigned to the π–π* transition of the aromatic groups. According to Dexter's exchange-energy-transfer theory, the luminescence intensity of hybrid materials depends on the energy matching degree between the triplet state of the ligand and the resonance-energy level of the central lanthanide ion [36]. Consequently, it can be predicted that the energy-levels-matching degree between DBM-Si and the Eu^{3+} ion is suitable, which resulted in the organic ligand being able to absorb abundant enough energy in the ultraviolet–visible range to transfer the energy to the corresponding Eu^{3+} ion [35].

Luminescence measurements have been carried on the Eu(III)-complex-functionalized VTES/TEOS composite hybrid materials at room temperature. The excitation spectra of samples A–D and pure $[(C_2H_5)_4N][Eu(DBM)_4]$ (P) (detected at 611 nm) and the UV–vis absorption spectrum of DBM-Si are presented in Fig. 4. There exists a large overlap between the excitation spectra of all the samples and the absorption spectrum of DBM-Si, indicating that the central Eu^{3+} ion in all the samples can be efficiently sensitized by the antenna ligand of DBM-Si [37–40]. Aiming at further investigation of this efficient ligand-to-metal-ion energy transfer, the energy difference between the triplet states of ligand DBM-Si and the resonance-energy level of the central Eu^{3+} ion is also researched. Based on the energy-transfer and intramolecular energy-transfer mechanisms, the intramolecular energy-transfer efficiency is the most important factor influencing the luminescence properties of rare-earth complexes [41–44]. It depends chiefly on two energy-transfer processes: the first leads from the triplet level of ligands to the emissive energy level of the Eu^{3+} ion by Dexter's resonant-exchange interaction [36]; the second is just an inverse energy transfer by a thermal deactivation mechanism. According to this theory, the conclusion can be drawn that energy differences have opposite influence on the two energy-transfer processes, and an optimal value can be assumed to exist. Sato et al. reported that too large or too small energy differences decrease the efficiency of the ligand-to-metal energy transfer [39,41–44]. The suitable energy difference for an efficient ligand-to-Eu^{3+}-ion intramolecular energy transfer lies in the range of 500–2500 cm^{-1} [41]. Fig. 5 shows the phosphorescence spectra of Gd-DBM-Si, using the fact that Gd^{3+} ion does not have energy levels in the visible part of the electromagnetic spectrum and therefore is an ion suitable to check the excited energy levels of the ligands. The triplet-state energy level is determined from the corresponding shortest-wavelength phosphorescence band (20,040 cm^{-1}), which is assumed to be the 0–0 transition of the ligand. The energy difference between the lowest triple-state energy of the modified ligand DBM-Si (20,040 cm^{-1}) and the resonance-energy levels of the Eu^{3+} ion ($^5D_1$, 19,020 cm^{-1}) [45,46] was calculated. Based on the value of the energy difference (1020 cm^{-1}), the conclusion can be drawn that the ligand DBM-Si can effectively sensitize the central Eu^{3+} ion in the VTES/TEOS composite hybrid materials.

As shown in Fig. 4, all of the excitation spectra consist of a very broad band instead of the characteristic narrow band of Eu^{3+} (395 nm), which indicates that the europium complex has been synthesized by an *in situ* technique via a sol–gel process. In the pure complex, the broad excitation band extending from 300 to 500 nm appears, which can be assigned to the π–π* transitions of conjugated double bonds in the aromatic β-diketonate ligands [45]. Compared with $[(C_2H_5)_4N][Eu(DBM)_4]$ (P), the maximum excitation wavelengths of the samples (A–D) show a small blue shift from about 414 to 400 nm, which implies that the local symmetry of the europium complex deceases in the VTES/TEOS composite xerogels [11].

The emission spectra of all the samples are given in Fig. 6, and the detailed luminescence data are shown in Table 1. From the emission spectra, characteristic emission peaks of the Eu^{3+} ion

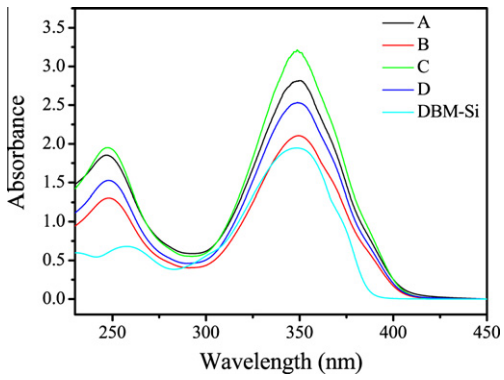

Fig. 3. UV–vis absorption spectra of DBM-Si and the samples A–D.

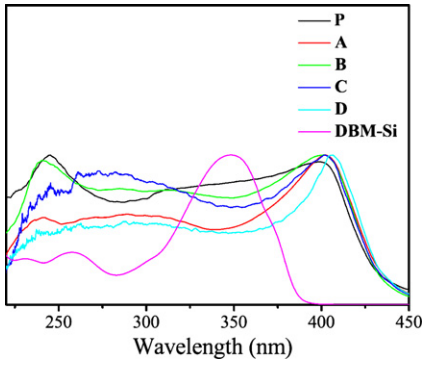

Fig. 4. The excitation spectra of $[(C_2H_5)_4N][Eu(DBM)_4]$ (P), samples A–D (detected at λ_{em} = 611 nm) and UV–vis absorption spectrum of DBM-Si.

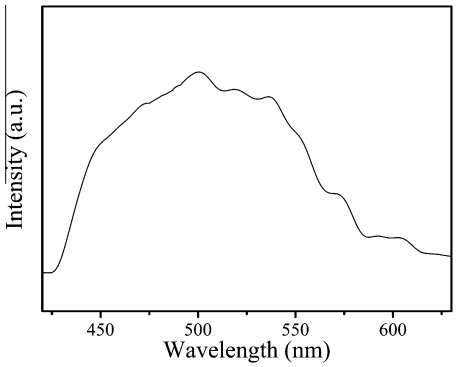

Fig. 5. Phosphorescence spectrum of $Gd(DBM\text{-}Si)_3{\cdot}2H_2O$ at 77 K. λ_{ex} = 355 nm.

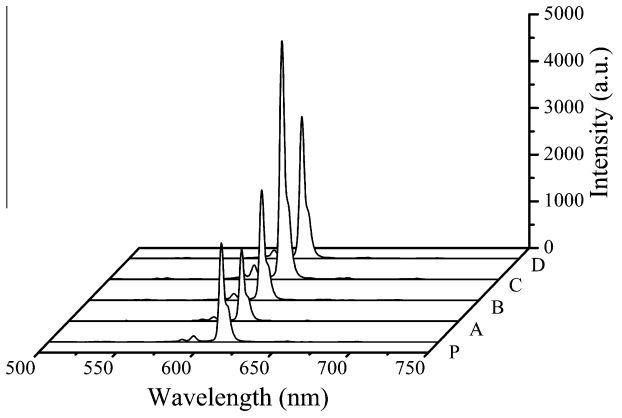

Fig. 6. The emission spectra of $[(C_2H_5)_4N][Eu(DBM)_4]$ (P), samples A–D. λ_{ex} = 400 nm.

Table 1
Luminescent efficiencies and lifetimes of europium covalent hybrids.

Systems	Pure Eu complex	Sample A	Sample B	Sample C	Sample D
υ_{00} (cm^{-1})[a]	17,059	17,059	17,059	17,059	17,059
υ_{01} (cm^{-1})[a]	16,858	16,858	16,858	16,858	16,858
υ_{02} (cm^{-1})[a]	16,361	16,361	16,361	16,361	16,361
υ_{03} (cm^{-1})[a]	15,305	15,305	15,305	15,305	15,305
υ_{04} (cm^{-1})[a]	14,331	14,331	14,331	14,339	14,331
I_{00}[b]	56.32	41.37	58.90	129.56	79.65
I_{01}[b]	132.16	89.16	136.56	292.73	175.38
I_{02}[b]	2119.82	1529.90	2355.74	5102.24	3037.58
I_{03}[b]	16.41	11.25	16.02	33.70	21.30
I_{04}[b]	6.66	5.19	7.50	17.15	10.05
I_{02}/I_{01}	16.04	17.16	17.25	17.43	17.32
A_{00} (s^{-1})	21.25	22.93	21.31	21.86	22.44
A_{01} (s^{-1})	50	50	50	50	50
A_{02} (s^{-1})	826.36	884.01	888.73	897.97	892.31
A_{03} (s^{-1})	6.84	6.95	6.46	6.34	6.69
A_{04} (s^{-1})	2.96	3.42	3.23	3.44	3.37
τ (ms)[c]	0.27	0.37	0.38	0.40	0.38
A_{rad} (s^{-1})	907.41	967.31	969.73	979.61	974.81
τ_{exp}^{-1}(s^{-1})	3703.70	2702.70	2631.58	2500.00	2631.58
A_{nrad} (s^{-1})	2796.29	1735.39	1661.85	1520.39	1656.77
η (%)	24.5	35.8	36.8	39.2	37.0

[a] Energies of the $^5D_0$–^7F_J transitions (υ_{0J}).
[b] Integrated intensity of the $^5D_0$–^7F_J emission curves.
[c] For $^5D_0$–^7F_J transition of Eu^{3+}.

are observed, which are assigned to the transitions $^5D_0$–$^7F_0$ (579 nm), $^5D_0$–$^7F_1$ (593 nm), $^5D_0$–$^7F_2$ (611 nm), $^5D_0$–$^7F_3$ (650 nm), and $^5D_0$–$^7F_4$ (700 nm). As is known, the $^5D_0$–$^7F_1$ transition corresponds to a parity-allowed magnetic dipole transition and is largely independent of the ligand field; therefore it can be used as an internal standard to account for the ligand differences [46]. The $^5D_0$–$^7F_2$ transition is a typical electric dipole transition and strongly varies with the local symmetry of Eu^{3+} ions. Among these transitions, the $^5D_0$–$^7F_2$ transition shows the strongest emission, suggesting that the chemical environment around the Eu^{3+} ions is in low symmetry [47,48]. It is interesting that a remarkable increase in fluorescent intensity was found with increasing addition of VTES in the bulk xerogels. As the VTES/TEOS molar ratio increases up to 4:6, the luminescent intensity of composite xerogels reaches a maximum, and it is enhanced by 3.3 and 2.4 times compared with TEOS-derived hybrid material and pure $[(C_2H_5)_4N][Eu(DBM)_4]$, respectively. Further increase of VTES results in a decrease of luminescent intensity. We attribute these results to three possible reasons. First, the surface Si–OH groups are replaced by Si–CH=CH_2 groups and their number decreases with increasing ratio of VTES to TEOS in the bulk xerogels, resulting in a subdued quenching effect between Eu(III) complexes and Si–OH. Second, Si–CH=CH_2 groups have an intense absorption band in the ultraviolet range, so they can absorb and transfer energy more effectively, which results in an increase of the luminescent intensity and quantum efficiency of VTES/TEOS composite hybrid materials. Finally, as the proportion of VTES increases, the surface hydrophobicity is enhanced over the inorganic TEOS xerogel, which effectively inhibits luminescence quenching by H_2O molecules [49]. But further improving hydrophobicity will not guarantee enough solubility for $[(C_2H_5)_4N][Eu(DBM)_3(DBM\text{-}Si)]$ in the ORMOSILs matrix and self-quenching between Eu(III) complexes in composite xerogels, which may decrease the emission efficiency [11]. Under our preparation conditions, the optimized molar ratio of VTES to TEOS is 4:6.

To study the thermal stability of photoluminescence, the temperature dependence of fluorescent intensity was measured under 325-nm excitation in various samples. The emission intensity of the $^5D_0$–$^7F_2$ transition for Eu^{3+} as a function of temperature is presented in Fig. 7. It is obvious that the variation of the emission intensity for the Eu^{3+} ions in hybrid materials shows a remarkable difference from that in the pure complex. The emission intensity of the $^5D_0$–$^7F_2$ transition for pure $[(C_2H_5)_4N][Eu(DBM)_4]$ decreases monotonically with increasing temperature in the studied range. However, for the hybrid materials, the emission intensity of $^5D_0$–$^7F_2$ transition, especially sample C, changes little at low temperature and then decreases quickly with the temperature increasing continuously. In Fig. 7, the intensity as a function of temperature is well fitted by the well-known thermal activation function [50]

$$I(T) = \frac{I_0}{1 + \alpha e^{-E_A/k_B T}}, \tag{1}$$

where I_0 is the emission intensity at 0 K, α is a proportionality coefficient, E_A is the thermal activation energy, k_B is the Boltzmann constant, and T is the absolute temperature. The values of E_A for the pure Eu(III) complex and samples A and C are determined to be 37.7, 55.8, and 76.0 meV, respectively. The improved values of E_A for the hybrid materials suggest that the thermal stabilities of the photoluminescence are much better than that of the pure complex. Furthermore, the VTES/TEOS composite hybrid material is most stable. It is suggested that, in the hybrid materials, because of the presence of ORMOSILs matrices, the vibrational transitions of the complexes are constrained, leading to improvement in the thermal stability of the photoluminescence [51].

The time-resolved intensity–decay curve of $^5D_0$–$^7F_2$ emissions for Eu^{3+} ions was measured at room temperature using a selective excitation wavelength of 355 nm, as shown in Fig. 8. All the decay

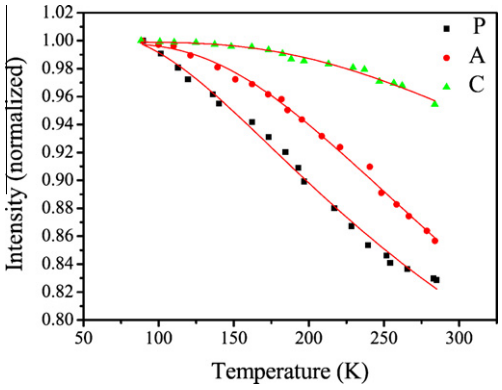

Fig. 7. Dependence of emission intensity of the $^5D_0$–$^7F_2$ on the temperature in samples P, A and C.

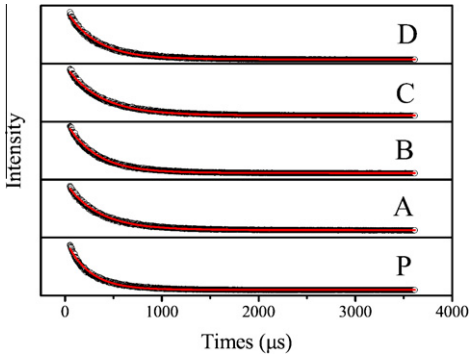

Fig. 8. Fluorescence decay dynamics of the $^5D_0$–$^7F_2$ transitions (λ_{em} = 611 nm) in various samples (room temperature).

curves can be described as a single exponential ($\ln(S(t)/S_0) = -k_1 t = -t/\tau$), indicating that all Eu^{3+} ions occupy the same average coordination environment. From the resulting lifetime data (shown in Table 1), it appears that the lifetimes of hybrid materials are longer than those of pure $[(C_2H_5)_4N][Eu(DBM)_4]$ (P). Moreover, the varying tendencies of hybrid material lifetimes are consistent with the order of the fluorescent intensity change; that is, with increasing addition of VTES in the bulk xerogels, the lifetime increases, and when the VTES/TEOS molar ratio increases to 4:6, the lifetime reaches a maximum. This may be attributed to two reasons. First, with increasing ratio of VTES to TEOS in the bulk xerogels, the surface Si–OH groups are replaced by Si–CH=CH_2 groups and their number decreases, which results in a subdued quenching effect between Eu(III) complexes and Si–OH. Second, the rigid Si–O and Si–C polymeric network restricts the vibration of the DBM ligand considerably and so improves the corresponding luminescence stability.

According to the emission spectrum and lifetime of the $^5D_0$ emitting level, the emission quantum efficiency (η) of the $^5D_0$ excited state of the europium ion for hybrid materials can be determined. If the process of the depopulation of the $^5D_0$ state is involved in nonradiative and radiative processes, η can be defined as how well the radiative processes compete with nonradiative processes [52],

$$\eta = \frac{A_r}{A_r + A_{nr}}, \tag{2}$$

where A_r and A_{nr} are radiative and nonradiative transition rates, respectively. Among these, nonradiative processes could influence the experimental luminescence lifetime, and could be described as follows [52–59]:

$$\tau_{exp} = (A_r + A_{nr})^{-1}. \tag{3}$$

So according to the radiative transition-rate constant and the experimental luminescence lifetime, quantum efficiency can be calculated from the following equation:

$$\eta = A_r \tau_{exp}. \tag{4}$$

Here A_r can be obtained by summing over the radiative rates A_{0J} for each $^5D_0$–^7F_J transition of Eu^{3+} [52–59]:

$$A_r = \sum A_{0J} = A_{00} + A_{01} + A_{02} + A_{03} + A_{04}. \tag{5}$$

The branching ratios for the $^5D_0$–$^7F_5$ and $^5D_0$–$^7F_6$ transitions can be neglected, as they are not detected experimentally. Therefore, we can ignore their influence on the depopulation of the $^5D_0$ excited state [52–59].

Since the $^5D_0$–$^7F_1$ transition is a magnetic-dipolar transition and is insensitive to the local structure environment around the Eu^{3+} ion, and thus can be considered as an internal reference for the whole spectrum, the experimental coefficients of spontaneous emission, A_{0J}, can be calculated according to the equation [52–59]

$$A_{0J} = A_{01}(I_{0J}/I_{01})(\upsilon_{01}/\upsilon_{0J}), \tag{6}$$

where υ_{01} and υ_{0J} are the energy barycenters of the $^5D_0$–$^7F_1$ and $^5D_0$–^7F_J transitions, respectively. A_{01} is Einstein's coefficient of spontaneous emission between the $^5D_0$ and $^7F_1$ energy levels. Since, in vacuum, the value of A_{01} can be determined to be approximately 50 s^{-1} ($A_{01} = n^3 A_{01(vacuum)}$) [15,59]. I is the emission intensity and can be taken as the integrated intensity of the $^5D_0$–^7F_J emission band [58,59]. Here the emission intensity, I, taken as the integrated intensity S of the $^5D_0$–$^7F_{0-4}$ emission curves, can be defined as

$$I_{i-j} = \hbar\omega_{i-j} A_{i-j} N_i \approx S_{i-j}, \tag{7}$$

where i and j are the initial ($^5D_0$) and final levels ($^7F_{0-4}$), respectively, ω_{i-j} is the transition energy, A_{i-j} is Einstein's coefficient of spontaneous emission, and N_i is the population of the $^5D_0$ emitting level. On the basis of the above discussion, we calculate the quantum efficiency of all the samples and list it in Table 1. As shown in Table 1, the quantum efficiencies of all the samples can be determined in the order sample C > sample B > sample D > sample A > pure Eu complex, which agrees with the order of lifetimes. From the equation for η, it can be seen η depends mainly on the values of two quanta: one is lifetime and the other is I_{02}/I_{01}. The ORMOSILs framework is a benefit for the luminescent properties of Eu^{3+} by increasing the ratio of radiative transition for the larger I_{02}/I_{01} ratio and longer lifetimes.

4. Conclusions

In summary, the Eu(III) complexes have been covalently immobilized by vinyl-modified silica networks through modification of *p*-hydroxydibenzoylmethane (DBM-OH) with 3-(triethoxysilyl)propyl isocyanate (TESPIC) using a sol–gel method. These materials display the connection of inorganic and organic parts on a molecular level due to the formation of an Si–O–Si network during cohydrolysis and co-condensation processes between the precursors, TEOS and VTES. The high hydrophobicity of the ORMOSILs and the more efficient energy absorption and transfer provided by VTES, acting as an organic modifier, results in enhanced luminescent intensity and emission quantum efficiency. At the optimal molar ratio of VTES to TEOS, the luminescent intensity of VTES/TEOS composite hybrid material is enhanced by 3.3 and 2.4 times compared with TEOS-derived hybrid material and pure $[(C_2H_5)_4N][Eu(DBM)_4]$, respectively. In addition, the thermo stability of the emission was also improved considerably. This improved performance of VTES/TEOS composite hybrid materials indicated that using vinyl-modified silicates as matrices could be expected to be a promising way to improve the properties of RE complexes.

Acknowledgment

The authors gratefully thank the National Natural Science Foundations of China (Grant 50872130).

Appendix A. Supplementary data

Supplementary data associated with this article can be found, in the online version, at doi:10.1016/j.jcis.2010.05.047.

References

[1] N. Sabbatini, M. Guardingli, J.M. Lehn, Coord. Chem. Rev. 123 (1993) 201.
[2] R. Reisfeld, Struct. Bonding 106 (2004) 209.

[3] G.F. DeSá, O.L. Malta, C.D. Donegá, A.M. Simas, R.L. Longo, P.A. Santa-Cruz, Chem. Rev. 196 (2000) 165.
[4] V.M. Mukkala, M. Helenius, J. Kankare, H. Takalo, Helv. Chim. Acta 76 (1993) 1361.
[5] J.C.G. Bünzli, C. Piguet, Chem. Rev. 102 (2002) 1897.
[6] M. Iwamuro, Y. Hasegawa, Y. Wada, K. Murakoshi, T. Kitamura, N. Nakashima, T. Yamanaka, S. Yanagida, Chem. Lett. 26 (1997) 1067.
[7] M.P.O. Wolbers, F.C.J.M. van Veggel, B.H.M. Snellink-Ruel, J.W. Hofstraat, F.A.J. Geurts, D.N. Reinhoudt, J. Chem. Soc. Perkin Trans. 2 (1998) 2141.
[8] J. Kido, Y. Okamoto, Chem. Rev. 102 (2002) 2357.
[9] M. Alvaro, V. Forns, S. Garca, H. Garca, J.C. Scaiano, J. Phys. Chem. B 102 (1998) 8744.
[10] D.J. Qian, H. Nakahara, K. Fukuda, K.Z. Yang, J. Colloid Interface Sci. 194 (1997) 174.
[11] Q.H. Xu, L.S. Li, X.S. Liu, R.R. Xu, Chem. Mater. 14 (2002) 549.
[12] C.Y. Peng, H.J. Zhang, J.B. Yu, Q.G. Meng, L.S. Fu, H.R. Li, L.N. Sun, X.M. Guo, J. Phys. Chem. B 109 (2005) 15278.
[13] B. Yan, Y. Li, B. Zhou, Microporous Mesoporous Mater. 120 (2009) 317.
[14] X.M. Guo, H.D. Guo, L.S. Fu, H.J. Zhang, R.P. Deng, L.N. Sun, J. Feng, S. Dang, Microporous Mesoporous Mater. 119 (2009) 252.
[15] R.F. de Farias, S. Alves Jr., M.F. Belian, G.F. de SáY, J. Colloid Interface Sci. 243 (2001) 523.
[16] Y. Li, B. Yan, Microporous Mesoporous Mater. 128 (2010) 62.
[17] P. Judeinstein, C. Sanchez, J. Mater. Chem. 6 (1996) 511.
[18] C. Sanchez, F. Ribot, L. Rozes, B. Alonso, Mol. Cryst. Liq. Crystallogr. 354 (2000) 731.
[19] C. Sanchez, B. Julian, P. Belleville, M. Popall, J. Mater. Chem. 15 (2005) 3559.
[20] P. Escribano, B. Julian-Lopez, J. Planelles-Arago, E. Cordoncillo, B. Viana, C. Sanchez, J. Mater. Chem. 18 (2008) 23.
[21] M. Pagliaro, R. Ciriminna, M. Wong Chi Man, S. Campestrini, J. Phys. Chem. B 110 (2006) 1976.
[22] L. Lin, L.L. Xiao, S. Huang, L. Zhao, J.S. Cui, Biosens. Bioelectron. 21 (2006) 1703.
[23] V.B. Kandimalla, V.S. Tripathi, H.X. Ju, Biomaterials 27 (2006) 1174.
[24] A. Fidalgo, R. Ciriminna, L.M. Iharco, M. Pagliaro, Chem. Mater. 17 (2005) 6686.
[25] Y. Xiong, J. Xu, J.W. Wang, Y.F. Guan, Anal. Bioanal. Chem. 394 (2009) 919.
[26] X. Wu, Y. Cong, Y. Liu, J. Ying, B. Li, J. Sol–gel Sci. Technol. 49 (2009) 355.
[27] P. Roche, R. Al-Jowder, R. Narayanaswamy, J. Young, P. Scully, Anal. Bioanal. Chem. 386 (2006) 1245.
[28] Y. Jiang, L.L. Xiao, L. Zhao, X. Chen, X. Wang, K.Y. Wong, Talanta 70 (2006) 97.
[29] B.J. Basu, Sens. Actuators B 123 (2007) 568.
[30] G. Qian, M. Wang, Z. Yang, J. Non-Cryst. Solids 286 (2001) 235.
[31] G. Qian, M. Wang, Z. Yang, J. Phys. Chem. Solids 63 (2002) 1829.
[32] G. Qian, Z. Yang, M. Wang, J. Lumin. 96 (2002) 211.
[33] B. Lei, B. Li, H. Zhang, L. Zhang, W. Li, J. Phys. Chem. C 111 (2007) 11291.
[34] H.R. Li, J. Lin, H.J. Zhang, H.C. Li, L.S. Fu, Q.G. Meng, Chem. Commun. 13 (2001) 1212.
[35] J.L. Liu, B. Yan, J. Phys. Chem. B 112 (2008) 10,898.
[36] D.L. Dexter, J. Chem. Phys. 21 (1953) 836.
[37] N. Sabbatini, A. Mecati, M. Guardigli, V. Balzani, J.M. Lehn, R. Zeissel, R. Ungaro, J. Lumin. 48 (1991) 463.
[38] M. Kawa, J.M.J. Fréchet, Chem. Mater. 10 (1998) 286.
[39] W.F. Sager, N. Filipescu, F.A. Serafin, J. Phys. Chem. 69 (1965) 1092.
[40] I.B. Berlman, Energy Transfer Parameters of Aromatic Compounds, Academic Press, New York, 1973.
[41] S. Sato, M. Wada, Bull. Chem. Soc. Jpn. 43 (1970) 1955.
[42] G.A. Crosby, R.E. Whan, R.M. Alire, J. Chem. Phys. 34 (1961) 745.
[43] B. Yan, H.J. Zhang, S.B. Wang, J.Z. Ni, J. Photochem. Photobiol. A Chem. 116 (1998) 209.
[44] X. Guo, H. Guo, L. Fu, H. Zhang, L.D. Carlos, R. Deng, J. Yu, J. Photochem. Photobiol. A Chem. 200 (2008) 318.
[45] S. Moynihan, D. Iacopino, D. O'Carroll, H. Doyle, D.A. Tanner, G. Redmond, Adv. Mater. 19 (2007) 2474.
[46] J.C.G. Bunzli, Luminescent probes, in: Lanthanide Probes in Life, Chemical and Earth Sciences, Theory and Practice, Elsevier, New York, 1989.
[47] P.J. Miranda, J. Zukerman-Schpector, P.C. Isolani, G. Vicentini, L.B. Zinner, J. Alloys Compd. 344 (2002) 141.
[48] X.M. Guo, L.S. Fu, H.J. Zhang, L.D. Carlos, C.Y. Peng, J.F. Guo, J.B. Yu, R.P. Deng, L.N. Sun, New J. Chem. 29 (2005) 1351.
[49] X. Chen, Z. Zhong, Z. Lia, Y. Jiang, X. Wang, K. Wong, Sens. Actuators B 87 (2002) 233.
[50] B.S. Li, Y.C. Liu, Z.Z. Zhi, D.Z. Shen, Y.M. Lu, J.Y. Zhang, X.W. Fan, J. Cryst. Growth 240 (2002) 479.
[51] Q. Li, T. Li, J. Wu, J. Phys. Chem. B 105 (2001) 12293.
[52] P.C.R. Soares-Santos, H.I.S. Nogueira, V. Félix, M.G.B. Drew, R.A.S. Ferreira, L.D. Carlos, T. Trindade, Chem. Mater. 15 (2003) 100.
[53] M.H.V. Werts, R.T.F. Jukes, J.W. Verhoeven, Phys. Chem. Chem. Phys. 4 (2002) 1542.
[54] L.D. Carlos, Y. Messaddeq, H.F. Brito, R.A.S. Ferreira, V.D.Z. Bermudez, S.J.L. Ribeiro, Adv. Mater. 12 (2000) 594.
[55] E.E.S. Teotonio, J.G.P. Espinola, H.F. Brito, O.L. Malta, S.F. Oliveria, D.L.A. de Faria, C.M.S. Izumi, Polyhedron 21 (2002) 1837.
[56] S.J.L. Ribeiro, K. Dahmouche, C.A. Ribeiro, C.V. Santilli, S.H.J. Pulcinelli, J. Sol–gel Sci. Technol. 13 (1998) 427.
[57] O.L. Malta, M.A.C. dosSantos, L.C. Thompson, N.K. Ito, J. Lumin. 69 (1996) 77.
[58] G.F. de Sa, O.L. Malta, C.D. Donega, A.M. Simas, R.L. Longo, P.A. Santa-Cruz, E.F. da Silva, Coord. Chem. Rev. 196 (2000) 165.
[59] J.C. Boyer, F. Vetrone, J.A. Capobianco, A. Speghini, M. Bettinelli, J. Phys. Chem. B 108 (2004) 20137.